Enhanced Lithium Storage Performance of CuO Nanowires by Coating of Graphene Quantum Dots

Chao, Dongliang; Zhu, Changrong; Sun, Jing; Bacho, Ignacio Mínguez; Fan, Zhanxi; Ng, Chin Fan; Xia, Xinhui; Huang, Hui; Zhang, Hua; Shen, Ze Xiang; Ding, Guqiao; Fan, Hong Jin

2014

https://hdl.handle.net/10356/79858

https://doi.org/10.1002/admi.201400499

Graphene Quantum Dots Coating Enhances Lithium Storage Performance of CuO Nanowires

Changrong Zhu, Dongliang Chao, Jing Sun, Ignacio Mínguez Bacho, Zhanxi Fan, Chin Fan Ng, Xinhui Xia, Hui Huang, Hua Zhang, Ze Xiang Shen, Guqiao Ding[*], and Hong Jin Fan[*]

C. Zhu, D. Chao, I. M. Bacho, C. F. Ng, Dr. X. Xia, Prof. Z. X. Shen, Prof. H. J. Fan
School of Physical and Mathematical Sciences, Nanyang Technological University, 637371, Singapore
Email: fanhj@ntu.edu.sg

J. Sun, Prof. G. Ding
State Key Laboratory of Functional Materials for Informatics, Shanghai Institute of Microsystem and Information Technology, Chinese Academy of Sciences, Shanghai 200050, People's Republic of China
Email: gqding@mail.sim.ac.cn

Z. Fan, Prof. H. Zhang
School of Materials Science and Engineering, Nanyang Technological University, 639798, Singapore

C. Zhu, Dr. H. Huang,
Singapore Institute of Manufacturing Technology, 71 Nanyang Drive, 638075 Singapore

C. Zhu and D. Chao contributed equally to this work.

Abstract

A new type of CuO/Cu/graphene quantum dots (GQDs) triaxial nanowires (referred as CCG) has been designed and successfully fabricated using a two-step electrochemical process followed by annealing. The synergistic combination of high-capacity metal oxide CuO and conductive layers of Cu and GQDs exerts an enhanced electrochemical performance for Li ion storage. The triaxial nanowire CCG electrode shows an improved reversible capacity (ca. 760 mAh g^{-1} cycled at 1/3 C) and rate capability (~60 % capacity retention cycled at 10 C) compared with nanowires without GQDs coating. A relatively high initial coulombic efficiency (~87 %) is obtained for the CCG anode as a result of the Cu and GQDs double layers. Meanwhile, the CCG anode showed high capacity retention in long cycles reached up to 1000 cycles. Enhancement mechanism is discussed. Our results demonstrate the effectiveness of GQDs coating in improving the electrochemical performance and stability of nanostructured electrodes for Li ion batteries and possibly also for other electrochemical devices.

Lithium-ion battery (LIB) has long been the dominating power source in the portable electronics market.[1] Nevertheless, the progress of LIB technology still falls behind the increasing industrial demands. Considerable research efforts have been dedicated in creating high-performance LIBs with high capacity, long life span, and enhanced rate capability.[2-8] Among the metal oxide anode materials, copper oxide (CuO) is considered as a promising candidate owing to its advantages such as high theoretical capacity (674 mAh g^{-1}), environmental benignity and low cost.

However, for the practical applications of CuO as LIBs anode, the large volume expansion (174 %),[9] low conductivity (p-type semiconductor), and subsequently particle pulverization problem remain the critical issues to be resolved. Nanostructures, heterostructures and surface coatings are main strategies to tackle with the CuO's deficiencies. A wide range of CuO nanostructures have been reported for LIB electrode application. They include dendrite-like,[10] hollow octahedra nanosphere,[11] nanoribbons,[12] 3D nanoporous,[13] flower-like microspheres,[14] and nanocrystalline-assembled bundle-like CuO nanostructure.[15] Although good electrochemical performance was demonstrated compared to bulk powder electrodes, the small cycle numbers (mostly below 100) are insufficient to evaluate its suitability for practical applications. Researchers have also tried to form heterostructures, such as CuO/Cu_2O,[16, 17] and Fe_3O_4/CuO hybrid wires[18] to improve the capacity, these composite nanostructure still suffer large volume expansion, low electric conductivity and poor cycling stability. Therefore, it is of great importance to introduce highly conductive and stable layer in fabricating long lifespan LIBs. It is noted that, attempts have been made in improving the performance of metal oxide based LIB electrodes by coating with carbon/polymer materials, such as PEDOTs,[19, 20] glucose,[21, 22] carbon nanotube,[23, 24] and graphene.[25]

The low initial coulombic efficiency (~35 %,[11, 26] ~65 %[12, 13, 15, 27-31]) is another critical issue for CuO as LIB anode. In the work of Cu_2O, researchers coated a conductive layer of Cu on the surface of Cu_2O nanoparticles and a higher (77%) coulombic efficiency was achieved.[32] We expect this approach is workable to CuO as well. But still the effectiveness of a single metallic Cu layer will weaken upon cycles due to the chemical/electrochemical corrosion in organic electrolyte. To further improve the structure stability and sustainability, coating materials with higher stability is needed, such as conductive carbon. As the emerging material, graphene quantum dots (GQDs) have the advantage of high solubility in various solvents by appropriate functionalization,[33, 34] and the capability of conformal wrapping on

low-dimensional nanostructures as a conductive layer by applying electrophoresis.[35] It is also expected that the GQDs coating decrease the electrochemical impedance and thus facilitates the transport kinetics. So far, chemically modified GQDs have been applied in solar cells,[36-38] oxygen reduction reaction electrodes,[39] supercapacitors,[35] and bio-analysis and sensors.[40] However, to our best knowledge, there has been no report on the application of GQDs for LIBs electrodes.

Herein, we have designed and synthesized successfully CuO+Cu+GQDs (referred as CCG) triaxial nanowire arrays for performance improvement as LIB anode. By comparing to un-protected CuO+Cu (referred as CC) core/shell nanowire electrodes, the unique GQDs soft protection shows greatly increased surface conductivity and the stability of nanowire array structure. As a result, the CCG anode delivers a high rate capability and excellent long term (up to 1000) cyclability. Our result demonstrates a new approach to enhance the performance of battery electrodes, particularly those materials that are unstable in electrolytes or have high lithiation-induced volume expansion (such as Sn or SnO_2, Si).

Fabrication and characterization of triaxial CuO/Cu/GQD nanowire electrodes

Figure 1 illustrates the entire fabrication process from growth of $Cu(OH)_2$ nanowires precursor to CuO nanowires and finally to CC and CCG nanowires (see sample color change in Fig. S1, Supporting Information). $Cu(OH)_2$ nanowires are first fabricated through electrochemical anodization of Cu foam (Fig. S1a). By annealing the $Cu(OH)_2$ nanowires at 200 ºC in air for 2 h (Fig. S1a-b), pure CuO nanowires are obtained (Fig. 1b). After further annealing under Ar+H_2 atmosphere for 0.5 h, the CuO nanowires can be transferred to CuO+Cu coaxial nanowires (Route 1 in Fig. 1b-c). The fabrication process of CCG triaxial nanowires is illustrated in Route 2 where a process of 10 min electrophoresis was employed prior to the annealing in Ar+H_2. Detailed illustration of the change from $Cu(OH)_2$ single

nanowire to CCG triaxial nanowire is shown in Fig. 1f, where three layer of CuO, Cu and GQDs can be easily seen for the final heterostructure.
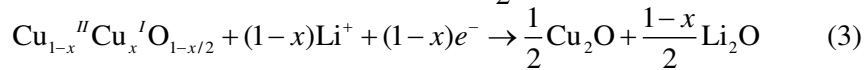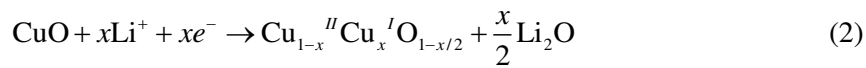
The corresponding scanning electron microscopy (SEM) images of the samples at different stages are shown in Fig. 2. The anodized precursor $Cu(OH)_2$ nanowires have a diameter of ca. 100 nm and a length of 1.5 µm (Fig. 2a). After annealing in air, the obtained CuO nanowires have rough surfaces but the nanowire array structure is maintained (Fig. 2b). As shown in Fig. 2c, the surface of CCG triaxial nanowires becomes mossy after the coating of an outer layer of GQDs. Meanwhile, the $Ar+H_2$ annealing converts a thin surface layer of CuO to metal Cu due to reduction reaction. As for the control sample of CuO+Cu coaxial nanowires (Fig. 2d), it is interesting to see that they are smoother than the CCG nanowires (as seen also by TEM images below). In nanoarchitectural engineering, rough surface indicates large specific surface area and more connection points for the electrochemical reactions. This implies that the CCG layer coating may contribute to extra capacity compared to the smooth CC nanowire anode.

To provide further insights to the microscopic structure of the coaxial and triaxial nanowires, transmission electron microscopy (TEM) investigations were performed. First, Fig. 3a shows a representative low-magnification TEM image of the GQDs and the corresponding size distribution (Inset). The GQDs are well dispersed in solution and thus also uniformly distributed on the TEM carbon film without commonly observed aggregation. The size of GQDs is peaked around 2-3 nm. The HRTEM (Fig. 3b) shows the lattice spacing of 0.21 nm related to the (1100) lattice plane of GQDs which is also detected in Fig. 3c. For the final CCG triaxial nanowire (Inset of Fig. 3c), a mossy morphology is observed, as consistent with the SEM image in Fig 2c. In addition to carbon (1100) lattice, the lattice planes of Cu (011) and CuO (111) are also clearly resolved in the HRTEM of CCG (Fig. 3c). In Fig. 3d, the HRTEM image of coaxial CC nanowires shows the lattices of Cu (011) and CuO (111)

5

only. Inset in Fig. 3d indicates a smooth layer of Cu ca. 15 nm. TEM mapping (Fig. 3e) illustrates the element distribution of O, Cu and C, respectively. It can be seen that the profile of O is slightly narrower than those of Cu and C, while the profile of Cu is nearly identical to that of C. This demonstrates unambiguously the formation of a uniform CuO+Cu+GQD triaxial sandwich structure. More evidence about the phase and composition of the products are provided by the X-ray diffraction (XRD), Raman, and X-ray photoelectron spectroscopy (XPS) results (see Fig. S2, S3 and the associated discussion in the Supporting Information). Therefore, it can be concluded that we have successfully fabricated the integrated electrode that contains uniform triaxial nanowires fully covering the copper foam surfaces.

Electrochemical property as LIB anode

To verify the advantage of our structure design, we conducted the characterization of the electrochemical properties of both the triaxial CCG nanowire and coaxial CC nanowire anodes. In Fig. 4a, the three cathodic peaks located at 1.8, 1.25 and 0.78 V correspond to the three sloping discharge potential plateaus (Fig. 4c) of 2.0–1.5 V, 1.5–1.01 V and 1.01–0.01 V of CCG nanowires anode, respectively. These peaks correspond to the formation of $Cu_{1-x}^{II}Cu_x^{I}O_{1-x/2}$, Cu_2O and Cu as shown in the follow equations:[30, 41]

$$CuO + 2Li^+ + 2e^- \leftrightarrow Cu + Li_2O \tag{1}$$

$$CuO + xLi^+ + xe^- \rightarrow Cu_{1-x}^{II}Cu_x^{I}O_{1-x/2} + \frac{x}{2}Li_2O \tag{2}$$

$$Cu_{1-x}^{II}Cu_x^{I}O_{1-x/2} + (1-x)Li^+ + (1-x)e^- \rightarrow \frac{1}{2}Cu_2O + \frac{1-x}{2}Li_2O \tag{3}$$

$$\frac{1}{2}Cu_2O + Li^+ + e^- \rightarrow Cu + \frac{1}{2}Li_2O \tag{4}$$

Equation (1) is the overall reaction during lithiation progress which can be divided into three sub-procedures as shown in Eq. (2–4). Two anodic peaks of 1.52 and 2.51 V correspond to

two sloping potential plateaus of 0.01–1.75 and 1.75–2.8 V related to the formation of Cu_2O and CuO.[31]

The trilayer CCG electrode exhibits an improved rate property compared to the coaxial CC electrode. As seen from Fig. 4b, the specific capacity for the CCG triaxial nanowires electrode ranges from 780 mAh g^{-1} at 1/3 C (1 C = 674 mA g^{-1}) to 330 mAh g^{-1} at 30 C. Comparatively, CC coaxial nanowires electrode shows a specific capacity ranging from 690 mAh g^{-1} at 1/3 C to 200 mAh g^{-1} at 30 C. The capacity decay of CCG anode is much less than that of CC anode. It is also noted that CCG triaxial nanowires electrode shows a better rate capacity recovery (~85 %) than the CC coaxial one (~70 %) after being cycled at a high current density of 30 C.

For CuO related electrodes, in general the initial coulombic efficiency has been low due to the formation of SEI and a relatively big volume expansion (174 %) of CuO. In our design, the metallic Cu layer may protect the inner CuO and suppress the SEI formation during the 1st discharge process (CuO → Cu). Meanwhile, this Cu layer can also release capacity (Cu → CuO) gradually in the following charge process. In addition, the outer GQDs layer can further protect the activity material from forming SEI layers especially during the first discharge process. Hence, the initial coulombic efficiency of our trilayered CCG electrodes can be radically improved compared to bare CuO: 82 % for CC coaxial nanowires electrode and 87 % for CCG triaxial nanowires electrode.

As the charge-discharge curves provide information on cycling stability, we illustrate the charge-discharge curves for both CCG and CC electrodes for 1st, 2nd, 100th, 300th and 500th cycles (Fig. 4c and 4d). As can be seen, the discharge curve at 500th cycle remains almost identical with that at 100th cycle, indicating the good cycling stability of our materials. It is obviously that the charge/discharge plateau of CCG electrode is much stable than that of CC

anode, suggesting the better electric conductivity and less electrochemical polarization of CCG triaxial electrode. This can also be proven by Nyquist plots of CCG and CC electrodes before and after 500 cycles (Fig. 4e and f). The resistance is simulated using equivalent circuit of $R_S(Q(R_{ct}Z_W))$, where R_S is the ohmic resistance of solution and electrodes; R_{ct} is the charge transfer resistance; Q is the double layer capacitance and Z_W is the Warburg impedance. It can be found by the simulated values that both the resistance of CC (285 Ω) and CCG (108 Ω) after 500 cycles are larger than the initial ones (75 Ω for CC and 50 Ω for CCG). Under both conditions, the CCG anode shows lower charge transfer resistances (before cycling: R_{ct} value is 35 for CCG sample while 72 for CC sample. After cycling: R_{ct} value is 119 for the CCG anode while 291 for the CC anode). This indicates a faster surface charge transfer process and higher Li^+ ion diffusing efficiency in the CCG electrode.[42]

The long-term cycling properties were also characterized for both electrodes in parallel at the same current densities to demonstrate the positive role of GQDs in nanostructure stabilization. Fig. 4g displays the cycling performance comparison between CCG and CC nanowire electrodes with a current density of 1/3 C for the first 500 cycles and 4C for the second 500 cycles. One can see that the CC coaxial nanowires anode undergoes a fierce capacity drop (ca. 35 %) during the first 80 cycles, while the CCG nanowires anode shows improved stability with less than 20 % capacity drop after even 300 cycles. Sharp capacity drop has also been observed in previous studies, which could be due to a poor electric conductivity and/or decomposition of the active materials.[11, 12, 43] A careful inspection of Fig. 4g shows that in further cycles (> 200), the capacity increases slightly. The capacity increase has been observed for many metal oxides such as CuO,[30] SnO_2[44] and Fe_3O_4.[45] It was proposed that the additional capacity can result from some side reactions forming LiOH, Li_2O and LiH during lithiation.[46] Another possible reason in our case is the oxidation of Cu shell to CuO during charge processes, and the CuO can also serve as fresh active material

contributing to the capacity. During the following cycles (> 500 cycles) at higher current density (4C), the capacity of CC electrode starts to fade. In contrast, the GQD-protected electrode maintains its discharge capacity all the way to 1000 cycles. The capacity fading for the CC electrode may be caused by the further volume expansion and decrease of the electric conductivity after the consumption of the metal Cu shell. As for the ultrastable CCG electrode, the GQDs provide surface protection that can simultaneously accommodate the volume expansion and contribute to its good electrical conductivity. Indeed, SEM images of the electrodes after 500 cycles (Fig. S4a, b) show that the CCG nanowire array structure is well preserved whereas the CC nanowires have serious aggregation most likely due to irreversible expansion. To demonstrate the universality of this method, other copper substrates such as Cu foam, Cu net and Cu foil were also applied for the growth. As shown in Fig. S5, homogeneous CCG nanoarrays were obtained on all these substrates.

Finally, we propose some possible advantages of our CuO-based trilayer nanoarray structure particularly the GQDs coating that account for the improved electrochemical performance. As reported earlier,[32] a Cu surface layer can have a passivation effect. In our experiment, the thin Cu layer was generated from the CuO nanowire itself by a low-temperature reduction annealing. So there exists a chemical binding between Cu and the CuO core, which ensures a good conductivity between electrolyte and the active material (viz., CuO core), resulting in high rate capacity. In addition, during the first charge process, the Cu layer can be anodized to CuO leading to an increase in the initial coulombic efficiency. As for the GQDs, the thin carbon layer may have served as a mechanically soft and electrically conductivity "armor" that can reduce the electrode polarization (supported by GV data) and increase the charge collection efficiency (supported by the EIS data), as well as preserve the structural integrity of each CuO nanowire. In addition, the GQD layer can also contribute to the high initial coulombic efficiency by preventing the thick solid electrolyte interfaces (SEI)

layer on pure CuO and Cu. As a result, the whole trilayer nanowire electrode can maintain its capacity in longer cycles than ever.

In conclusion, a novel copper oxide/Cu/graphene quantum dots (CuO/Cu/GQD) triaxial nanowires electrode has been developed for their application in Li ion storage. This is the first time that GQDs is applied in surface engineering of LIB electrode. Such integrated electrodes exhibit ultrafast and ultrastable Li ion storage performance, with higher capacities and improved rate and cycling stability than the nanowires without GQDs. Owing to the unique Cu and GQDs double layer enhancement, the CCG triaxial nanowire electrodes show high capacity retention in first 100 cycles and nearly no capacity decay afterwards until 1000 cycles. A high rate capability recovery is achieved even after cycled at 30 C. Furthermore, the achieved high initial coulombic efficiency (ca. 87%) can be ascribed to a synergetic contribution from the Cu and GQDs layers. This work paves the way for GQDs applications in electrode materials for LIB as well as other rechargeable batteries.

Experiment

Synthesis of graphene quantum dots (GQD)

GQDs were prepared from graphene powder via a modified Staudenmaier method. Graphene powder (4 g) was put into H_2SO_4 (150 mL) and HNO_3 (80 mL) with stirring at 15 °C, and was kept for 2 h. Then $NaClO_3$ (40 g) was added gradually and the temperature was kept below 5 °C. The mixture was then stirred at 15 °C for 5 h. After that, the reaction was terminated by adding distilled water (80 mL). The PH value was neutralized to 7 by NaOH, before the mixture was filtered out using an alumina inorganic membrane with 20 nm pores. The obtained light yellow filtrate was dialyzed in a 3500 Da dialysis bag against deionized water for a week to remove excess salt. The purified solutions were transferred to a Teflon-lined autoclave and heated at 200 °C for 5 h to reduce the oxygen-containing groups, and cooling to room temperature naturally. The resultant light yellow solution of GQDs was obtained.

Synthesis of CC and CCG nanowires

All reagents were analytically pure and used without further purification. Compressed Cu foams were cut into standard pieces (1×1 cm^2) with a small rectangle holder (0.4×1 cm^2) at the middle of one side acting as the connection part (see supporting information Figure S1). The substrates were washed in acetone, ethanol and distilled water for 20 min separately and then dried with N$_2$ gun. After that, the back side of the substrate was covered with tape, and anodization was conducted in 1M NaOH with a CHI 760d using chronopotentiometry technique under 10 mA anodizing current for 10 min. After anodization, the surface of the substrates turned into pure blue Cu(OH)$_2$ nanowires. The samples were then annealed in air under 200 ^{o}C for 2 h, in which the which Cu(OH)$_2$ transformed to CuO. The GQDs were dispersed in DI water and then anchored to the CuO nanowire surfaces with an electrophoresis process under a constant direct voltage of 6 V for 10 min (CuO as working electrode and platinum as counter electrode). The samples were then annealed in Ar+5% H$_2$ (1.3 slm (standard liters per minute)) for 30 min under 200 ^{o}C, after which the final CuO+Cu+GQDs triaxial structure was formed. The control sample of CuO+Cu coaxial nanowires was synthesized by annealing the CuO nanowires under the same condition.

Structure and morphology characterization

The crystal structures of the samples were identified using X-ray diffraction (XRD, RigakuD/Max-2550 with Cu Kα radiation). Raman spectra were obtained with a WITec-CRM200 Raman system with a laser wavelength of 532 nm (2.33 eV). The Si peak at 520 cm^{-1} was used as a reference to calibrate the wavenumber. The as synthesized CCG triaxial nanowires were imaged by scanning electron microscopy (SEM JEOL 2100), and a high-resolution transmission electron microscopy (HRTEM, JEOL JEM-2010F) operating at 200 kV. The XPS measurements were performed with a VG ESCALAB 220i-XL system using a monochromatic Al Ka1 source (1486.6 eV).

Battery assembly and electrochemical test

After materials preparation, standard CR2032-type coin cells were assembled in an argon-filled glove box (Mbraun, Unilab, Germany) using the as-fabricated CCG nanowires or CC nanowires as the working electrode without any binder or additives, and the metallic lithium foil as the counter electrode. The electrolyte solution contained 1 M LiPF$_6$ in ethylene carbonate (EC)–dimethyl carbonate (DME) (1:1 in volume) and a polypropylene (PP) film (Cellgard 2400) was used as the separator. Galvanostatic charge discharge cycles were tested using Neware battery tester at different current densities between 0.01 and 3.0 V vs Li/Li$^+$ at room temperature. The CV measurements were carried out using a CHI-760d electrochemical work station at a scanning rate of 0.1 mV s^{-1} in the voltage range of 0.01–3.0 V. For electrochemical impedance spectroscopy (EIS), the amplitude of the sine perturbation signal was 5 mV, and the frequency was scanned from the highest (10 kHz) to the lowest (5 mHz).

To accurately determine the mass loading of the CC and CCG nanowire, the samples were weighed after each step using an analytical balance (d = 1 µg). The mass values are presented in Table S1 (Supporting Information). Through a careful calculation (see details in Supporting Information), the mass of CCG and CC are obtained to be 1.898 and 1.851 mg, respectively.

Reference and notes

[1]   J. B. Goodenough, K.-S. Park, *J. Am. Chem. Soc.* **2013**, *135*, 1167.

[2]   R. Mukherjee, R. Krishnan, T.-M. Lu, N. Koratkar, *Nano Energy* **2012**, *1*, 518.

[3]   L. Lu, X. Han, J. Li, J. Hua, M. Ouyang, *J Power Sources* **2013**, *226*, 272.

[4]   C.-M. Park, J.-H. Kim, H. Kim, H.-J. Sohn, *Chem Soc Rev* **2010**, *39*, 3115.

[5]   J. M. Tarascon, M. Armand, *Nature* **2001**, *414*, 359.

[6]   N. S. Choi, Z. Chen, S. A. Freunberger, X. Ji, Y. K. Sun, K. Amine, G. Yushin, L. F. Nazar, J. Cho, P. G. Bruce, *Angew Chem Int Ed Engl* **2012**, *51*, 9994.

[7]   X. Li, C. Wang, *J. Mater. Chem. A* **2013**, *1*, 165.

[8]   L. Ji, Z. Lin, M. Alcoutlabi, X. Zhang, *Energy Environ. Sci.* **2011**, *4*, 2682.

[9]   X. Wang, D.-M. Tang, H. Li, W. Yi, T. Zhai, Y. Bando, D. Golberg, *Chem. Commun.* **2012**, *48*, 4812.

[10]   C. Zhang, J. Chen, Y. Zeng, X. Rui, J. Zhu, W. Zhang, C. Xu, T. M. Lim, H. H. Hng, Q. Yan, *Nanoscale* **2012**, *4*, 3718.

[11]   R. Wu, X. Qian, F. Yu, H. Liu, K. Zhou, J. Wei, Y. Huang, *J. Phys. Chem. A* **2013**, *1*, 11126.

[12]   K. Chen, D. Xue, *Phys. Chem. Chem. Phys.* **2013**, *15*, 19708.

[13]   D. Liu, Z. Yang, P. Wang, F. Li, D. Wang, D. He, *Nanoscale* **2013**, *5*, 1917.

[14]   Z. Yuan, Y. Wang, Y. Qian, *RSC Adv.* **2012**, *2*, 8602.

[15]   L. Wang, W. Cheng, H. Gong, C. Wang, D. Wang, K. Tang, Y. Qian, *J. Mater. Chem.* **2012**, *22*, 11297.

[16]   J. Y. Zheng, T.-K. Van, A. U. Pawar, C. W. Kim, Y. S. Kang, *RSC Adv.* **2014**, *4*, 18616.

[17]   L. Hu, Y. Huang, F. Zhang, Q. Chen, *Nanoscale* **2013**, *5*, 4186.

[18]   S. Saadat, J. Zhu, D. H. Sim, H. H. Hng, R. Yazami, Q. Yan, *J. Phys. Chem. A* **2013**, *1*, 8672.

[19]   X. Xia, D. Chao, Z. Fan, C. Guan, X. Cao, H. Zhang, H. J. Fan, *Nano Lett.* **2014**, *14*, 1651.

[20]   D. Chao, X. Xia, J. Liu, Z. Fan, C. F. Ng, J. Lin, H. Zhang, Z. X. Shen, H. J. Fan, *Adv. Mater.* **2014**, 10.1002/adma.201400719.

[21]   C. Guan, Z. Zeng, X. Li, X. Cao, Y. Fan, X. Xia, G. Pan, H. Zhang, H. J. Fan, *Small* **2014**, *10*, 300.

[22]   Z. Zhang, R. Dua, L. Zhang, H. Zhu, H. Zhang, P. Wang, *ACS Nano* **2013**, *7*, 1709.

[23]   H. Huang, Q. Yu, Y. Ye, P. Wang, L. Zhang, M. Gao, X. Peng, Z. Ye, *CrystEngComm* **2012**, *14*, 7294.

[24]   Y. Xu, G. Jian, M. R. Zachariah, C. Wang, *J. Mater. Chem. A* **2013**, *1*, 15486.

[25]   L. Chen, M. Zhang, W. Wei, *J. Nanomater.* **2013**, *2013*, 1.

[26]   Y. Hu, X. Huang, K. Wang, J. Liu, J. Jiang, R. Ding, X. Ji, X. Li, *J. Solid State Chem.* **2010**, *183*, 662.

[27]   X. Chen, N. Zhang, K. Sun, *J. Mater. Chem.* **2012**, *22*, 13637.

[28]   F. Wang, W. Tao, M. Zhao, M. Xu, S. Yang, Z. Sun, L. Wang, X. Song, *J. Alloys Compd.* **2011**, *509*, 9798.

[29]   X. Xue, P. Deng, S. Yuan, Y. Nie, B. He, L. Xing, Y. Zhang, *Energy Environ. Sci.* **2013**, *6*, 2615.

[30]   J. Y. Xiang, J. P. Tu, Y. Q. Qiao, X. L. Wang, J. Zhong, D. Zhang, C. D. Gu, *J. Phys. Chem. C* **2011**, *115*, 2505.

[31]   X. Chen, N. Q. Zhang, K. N. Sun, *J. Phys. Chem. C* **2012**, *116*, 21224.

[32]   J. Y. Xiang, J. P. Tu, Y. F. Yuan, X. H. Huang, Y. Zhou, L. Zhang, *Electrochem. Commun.* **2009**, *11*, 262.

[33]   M. Bacon, S. J. Bradley, T. Nann, *Part. Part. Syst. Charact.* **2014**, *31*, 415.

[34]   Z. Zhang, J. Zhang, N. Chen, L. Qu, *Energy Environ. Sci.* **2012**, *5*, 8869.

[35]   W. Liu, X. Yan, J. Chen, Y. Feng, Q. Xue, *Nanoscale* **2013**, *5*, 6053.

[36]   M. Dutta, S. Sarkar, T. Ghosh, D. Basak, *J. Phys. Chem. C* **2012**, *116*, 20127.

[37]   P. Gao, K. Ding, Y. Wang, K. Ruan, S. Diao, Q. Zhang, B. Sun, J. Jie, *J. Phys. Chem. C* **2014**, *118*, 5164.

[38]   J. Tian, H. Zhao, X. Quan, Y. Zhang, H. Yu, S. Chen, *Sens. Actuators B: Chem.* **2014**, *196*, 532.

[39]   X. Zhou, Z. Tian, J. Li, H. Ruan, Y. Ma, Z. Yang, Y. Qu, *Nanoscale* **2014**, *6*, 2603.

[40]   A. Ananthanarayanan, X. Wang, P. Routh, B. Sana, S. Lim, D.-H. Kim, K.-H. Lim, J. Li, P. Chen, *Adv. Funct. Mater.* **2014**, *24*, 3021.

[41]   A. Débart, L. Dupont, P. Poizot, J. B. Leriche, J. M. Tarascon, *J. Electrochem. Soc.* **2001**, *148*, A1266.

[42]   C. Peng, H. Chen, Q. Li, W. Cai, Q. Yao, Q. Wu, J. Yang, Y. Yang, *J. Mater. Chem. A* **2014**, *2*, 13859.

[43]   J. Wang, Y. Liu, S. Wang, X. Guo, Y. Liu, *J. Mater. Chem. A* **2014**, *2*, 1224.

[44]   C. Zhu, X. Xia, J. Liu, Z. Fan, D. Chao, H. Zhang, H. J. Fan, *Nano Energy* **2014**, *4*, 105.

[45]   J. Luo, J. Liu, Z. Zeng, C. F. Ng, L. Ma, H. Zhang, J. Lin, Z. Shen, H. J. Fan, *Nano Lett.* **2013**, *13*, 6136.

[46]   Y.-Y. Hu, Z. Liu, K.-W. Nam, O. J. Borkiewicz, J. Cheng, X. Hua, M. T. Dunstan, X. Yu, K. M. Wiaderek, L.-S. Du, K. W. Chapman, P. J. Chupas, X.-Q. Yang, C. P. Grey, *Nat. Mater.* **2013**, *12*, 1130.
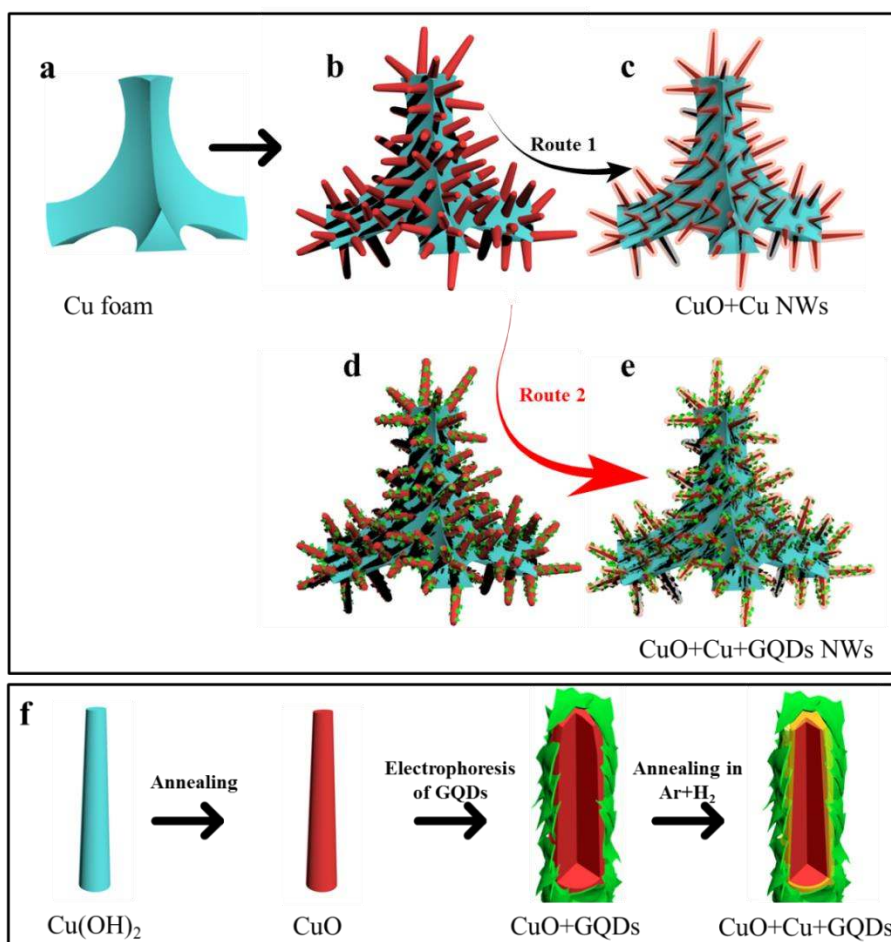
Figure 1. **Schematics of the fabrication process of CuO-based nanowire electrodes**. Route 1 for CuO+Cu (CC) core/shell nanowires. Route 2 for CuO+Cu+GQD (CCG) triaxial nanowires. (a) Pure copper foam. (b) CuO nanowire obtained by anodization followed by annealing in air at 200 °C. (c) CuO+Cu coaxial nanowires obtained after reduction annealing of b in an Ar + H_2 atmosphere at 200 °C. (d) CC core/shell nanowires after electrophoresis deposition of GQDs on b. (e) CCG triaxial nanowires obtained after reduction annealing of d in an Ar + H_2 atmosphere at 200 °C. (f) Detailed illustration of the fabrication process of CCG coaxial nanowires.

15
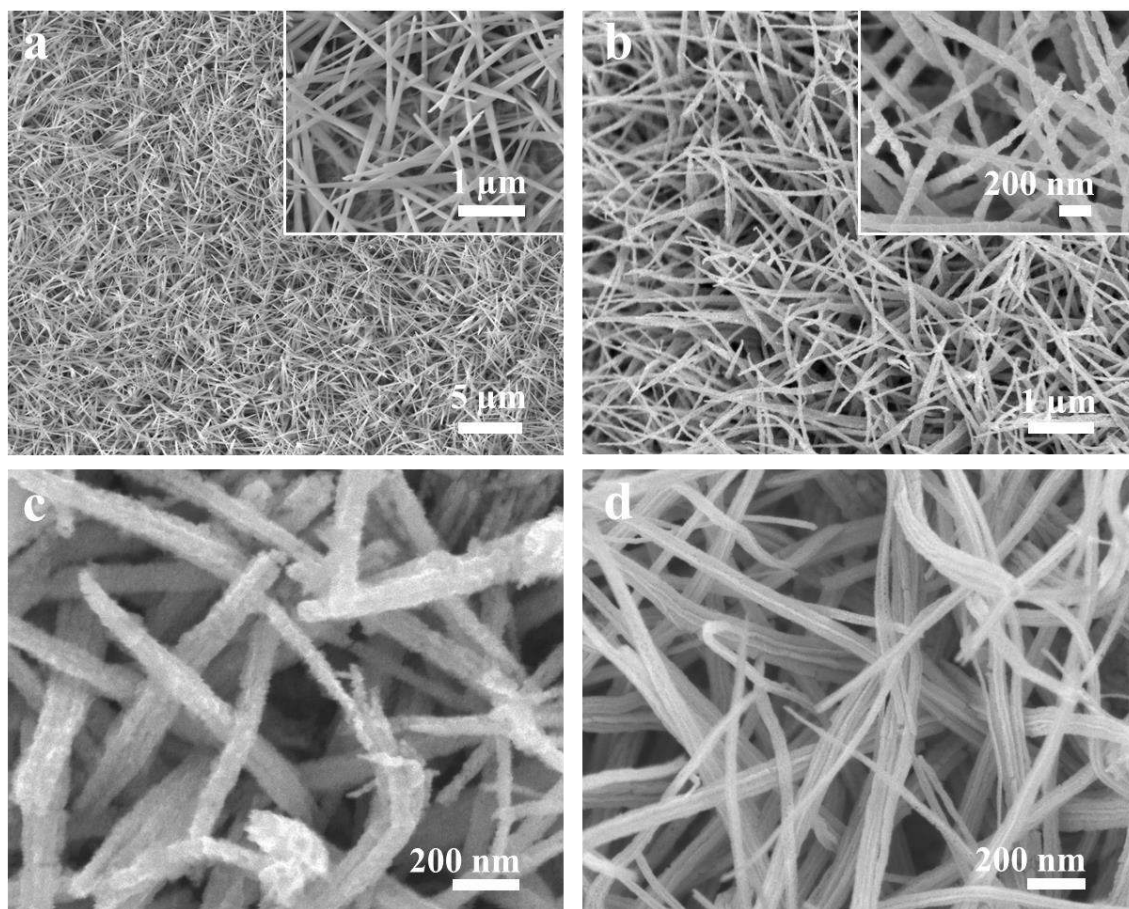
Figure 2. **SEM images of the nanowires at different fabrication stages.** (a) $Cu(OH)_2$ nanowires precursor. (b) CuO nanowires. (c) CuO+Cu+GQD triaxial nanowires. (d) CuO+Cu core/shell nanowires. Insets in a and b are the corresponding high magnification views.
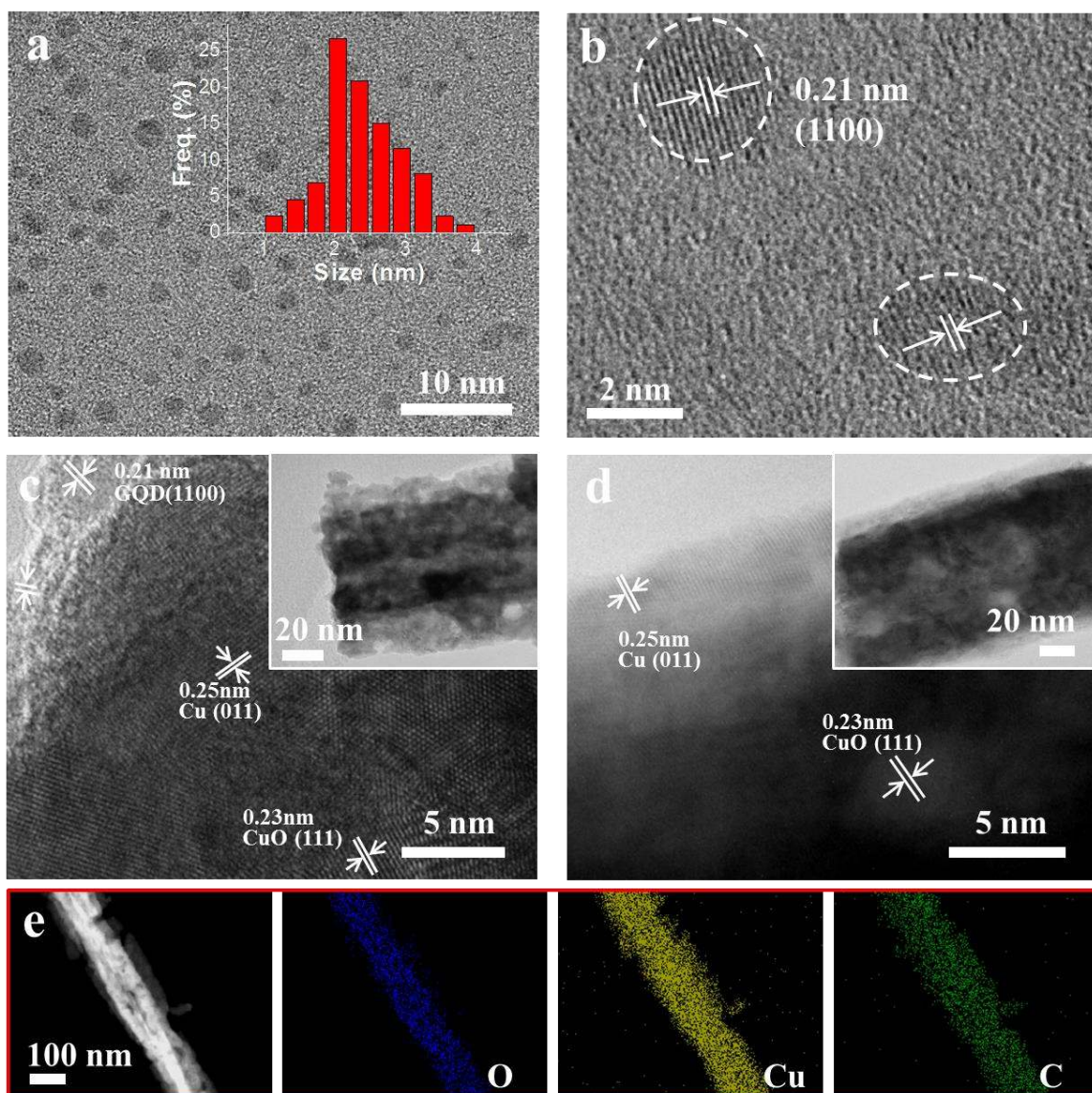
Figure 3. **TEM characterization of the GQDs and CuO-based nanowires.** (a) TEM image of as-synthesized GQDs. Inset is the corresponding size distribution obtained from TEM images. (b) HRTEM of two GQDs. (c) HRTEM image of CCG triaxial nanowire. Inset is a low-magnification view. (d) HRTEM image of CC core/shell nanowire. Inset is the low-magnification view. (e) Scanning TEM elemental mapping of the CCG triaxial nanowire.
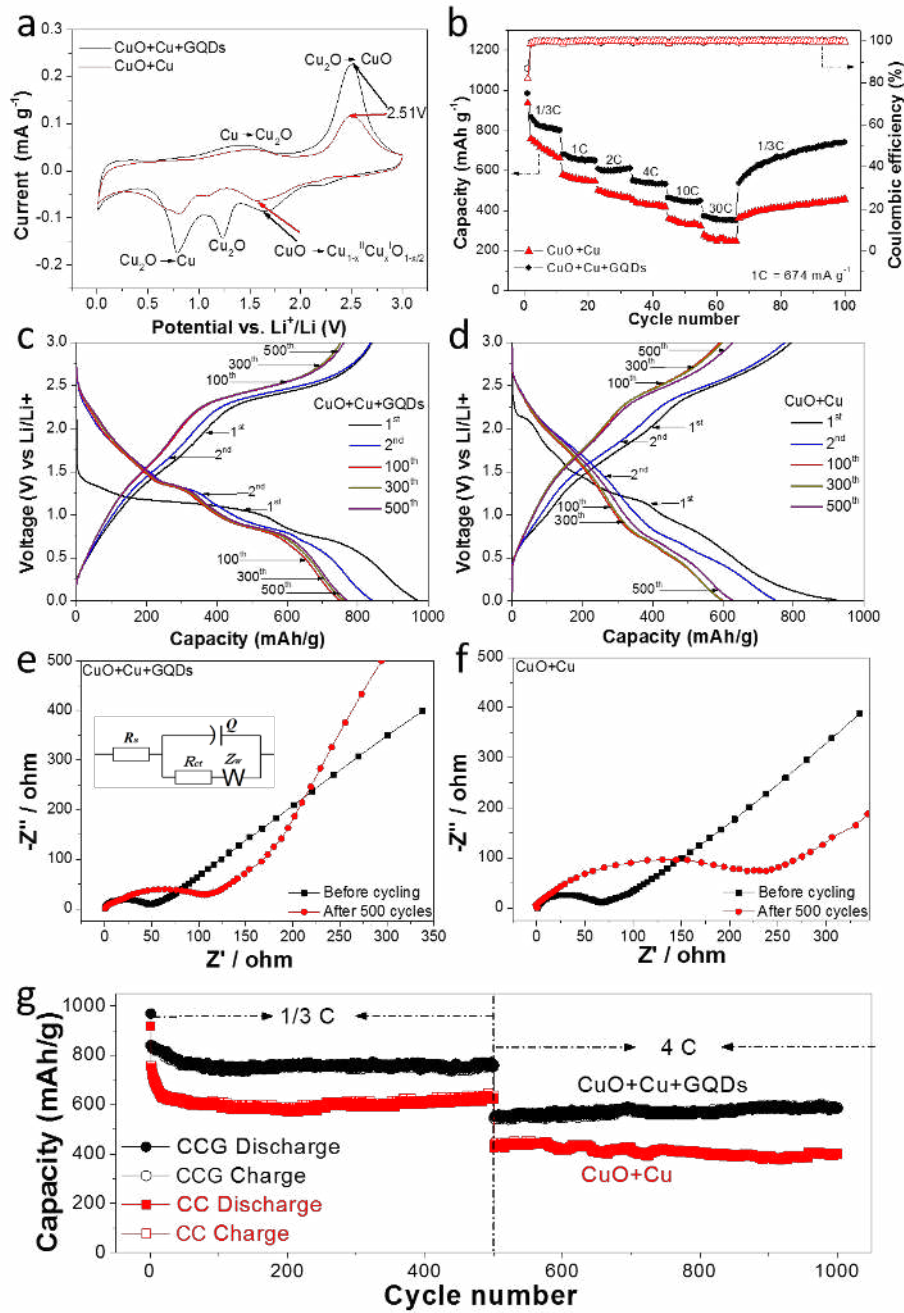
Figure 4. **Electrochemical characterization of CCG and CC anodes.** All specific capacities are calculated based on the total mass of the active materials (CuO, Cu and GQDs in the CCG and CC nanowires). (a) CV curve. (b) Rate performance with coulombic efficiency. (c, d) Discharge-charge curves (at a current density of 225 mA g^{-1}, 1/3 C) at different cycles for CCG and CC nanowire electrode, respectively. (e, f) Nyquist plots of CCG and CC nanowires electrodes before and after 500 cycles, respectively. Inset figure in e is the equivalent circuit of the CCG and CC anode. Rs: contact resistance; Rct: charge transfer resistance; Q: constant phase element (space double-layer capacitance); Zw: Warburg impedance. (g) Cycling performance at 1/3 C for the first 500 cycles and 4C for the second 500 cycles.

Graphene Quantum Dots Coating Enhances Lithium Storage Performance of CuO Nanowires

Changrong Zhu, Dongliang Chao, Jing Sun, Ignacio Mínguez Bacho, Zhanxi Fan, Chin Fan Ng, Xinhui Xia, Hui Huang, Hua Zhang, Ze Xiang Shen, Guqiao Ding[*], and Hong Jin Fan[*]

C. Zhu, D. Chao, I. M. Bacho, C. F. Ng, Dr. X. Xia, Prof. Z. X. Shen, Prof. H. J. Fan
School of Physical and Mathematical Sciences, Nanyang Technological University, 637371, Singapore
Email: fanhj@ntu.edu.sg

J. Sun, Prof. G. Ding
State Key Laboratory of Functional Materials for Informatics, Shanghai Institute of Microsystem and Information Technology, Chinese Academy of Sciences, Shanghai 200050, People's Republic of China
Email: gqding@mail.sim.ac.cn

Z. Fan, Prof. H. Zhang
School of Materials Science and Engineering, Nanyang Technological University, 639798, Singapore

C. Zhu, Dr. H. Huang,
Singapore Institute of Manufacturing Technology, 71 Nanyang Drive, 638075 Singapore

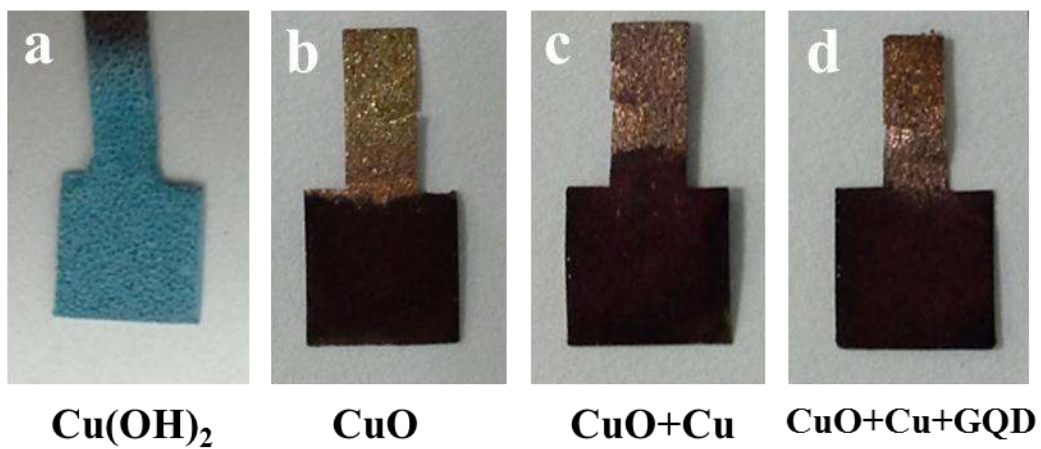C. Zhu and D. Chao contributed equally to this work.

Figure S1. Photographs of the sample at different fabrication stages.
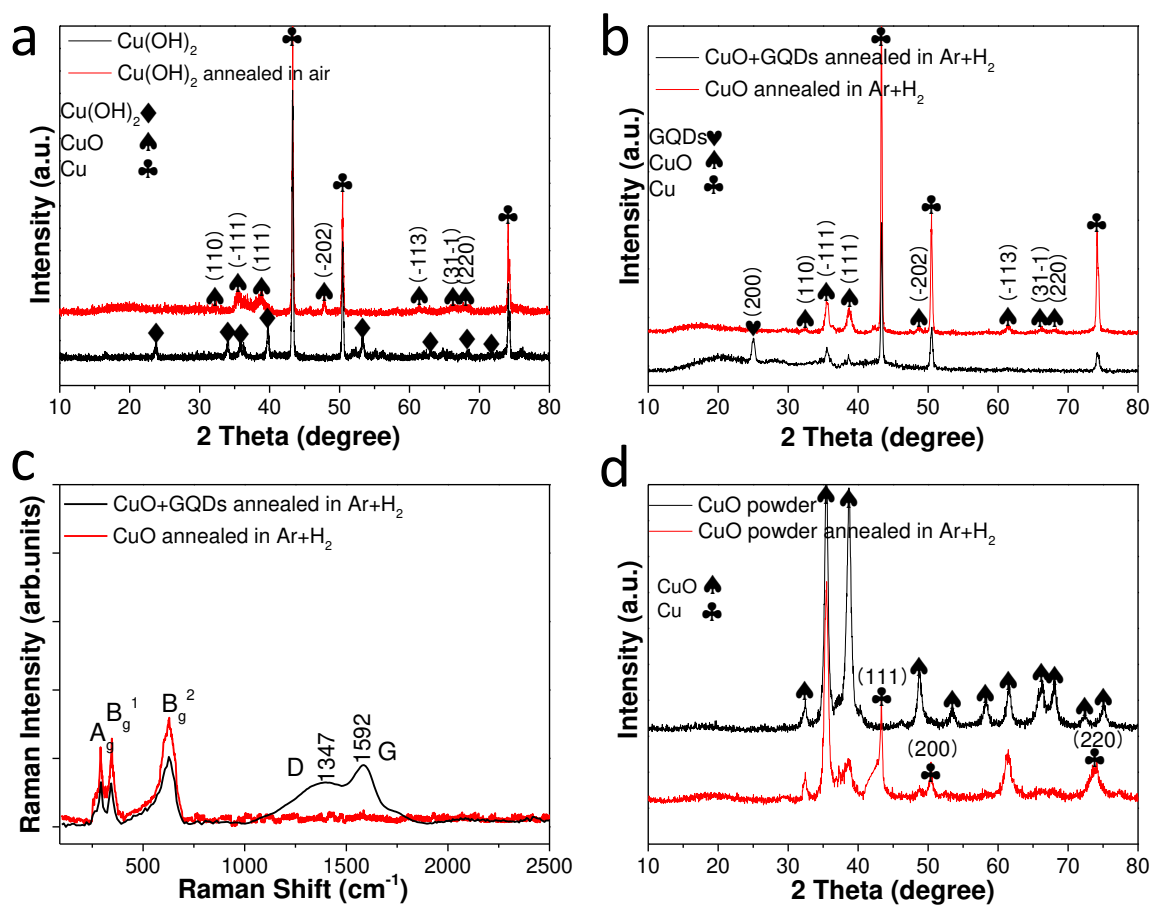
Figure S2. a) XRD pattern of anodized $Cu(OH)_2$ and CuO by annealing the $Cu(OH)_2$ nanowires in air under 200 °C for 2 h. b) XRD pattern of the CuO and CuO+GQDs annealed in Ar+H_2 under 200 °C for 0.5 h. c) Raman spectra of CC and CCG samples. d) XRD pattern of commercial nanosized-CuO powder and the powder after annealed in Ar+H_2 under 200℃ for 0.5h. This experiment (without Cu foam) was done in order to show more clearly the formation of Cu after reduction annealing.
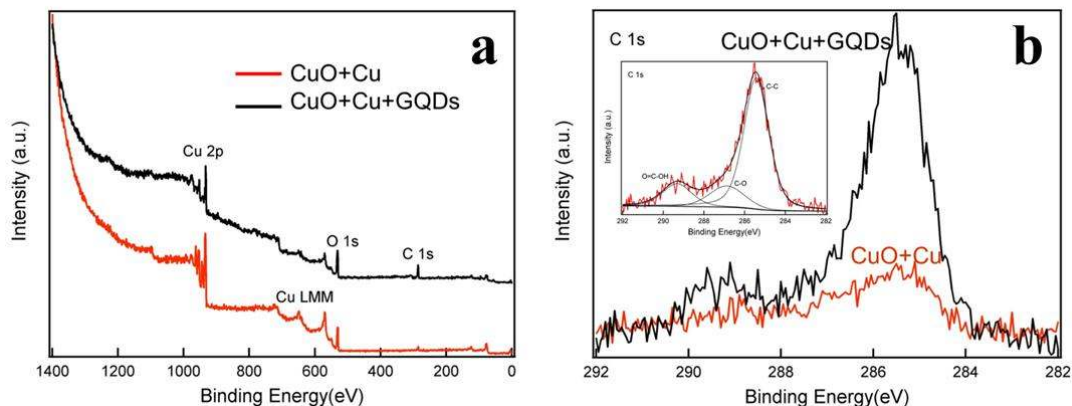
Figure S3. XPS pattern of sample CuO and CuO+GQDs annealed in Ar+H$_2$: a) Wide scan. b) C 1s peaks. Inset is the C 1s spectra from CCG triaxial nanowires with fitting results.

Discussion on XRD, Raman and XPS results (Figure S2, S3)

The X-ray diffraction (XRD) pattern is recorded directly from the sample on Cu foam substrate. The result shown orthorhombic Cu(OH)$_2$ phase (PDF#03-0315) before annealing, which were transferred to pure monoclinic CuO (PDF# 65-2309) during the annealing. In Fig. S2a, only the phases of CuO and Cu are detected after annealing, indicating the completely transfer of Cu(OH)$_2$ nanowires to CuO nanowires. After electrophoresis of GQDs, (200) lattice of GQDs can also be detected for the CCG sample (Fig. S2b). To further confirm the formation of Cu layer after the Ar + H$_2$ annealing and eliminate the signal from the Cu foam, we annealed commercial nanosized-CuO powder (ca. 50 nm) under the same annealing condition. The XRD patterns (Fig. S2d) show that Cu peaks (PDF#03-1005) indeed appear. In addition, the Raman spectra show clearly peaks of D band (1347 cm^{-1}) and G band (1592 cm^{-1}) from carbon (Fig. S2c). This certifies the existence of GQDs[1, 2] from the CCG nanowires. Meanwhile, the Raman spectra of both samples revealed three main phonon modes of CuO nanowire, at 291, 340 and 623 cm^{-1}, corresponding to the A$_g$, B$_g^1$ and B$_g^2$ symmetries[3-8], respectively.

From the wide scan XPS spectra of CC and CCG nanowires on Cu foam (Fig. S3a), it is obvious that C 1s peak intensity from CCG sample is much larger than that from CC, implying the existence of graphene. Also, the C 1s peak from the CCG sample is obvious stronger than that of CC. The weak C 1s signal of CC sample may come from the atmosphere and the carbon tape used in the testing process. The O 1s peak in Fig S3a is weak after annealing in Ar+H$_2$. This indicate low defect of GQDs and good structure maintain of graphite, which explains the high conductivity of the CCG anode. In Fig. S3b inset, the peaks of C 1s (C−C: 285.4 eV, C−O: 286.8 eV, O=C−OH: 289.3 eV)

correspond well with those of graphene-related materials[9, 10]. This is another proof of the successful coating of GQDs.
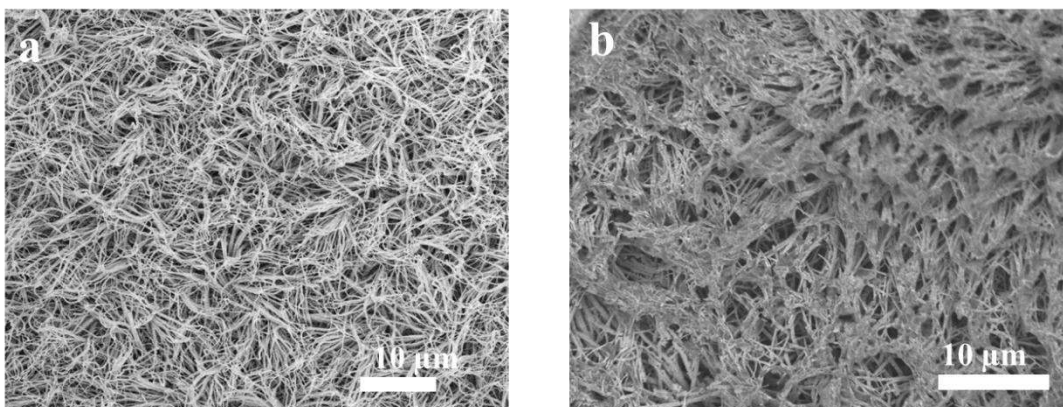

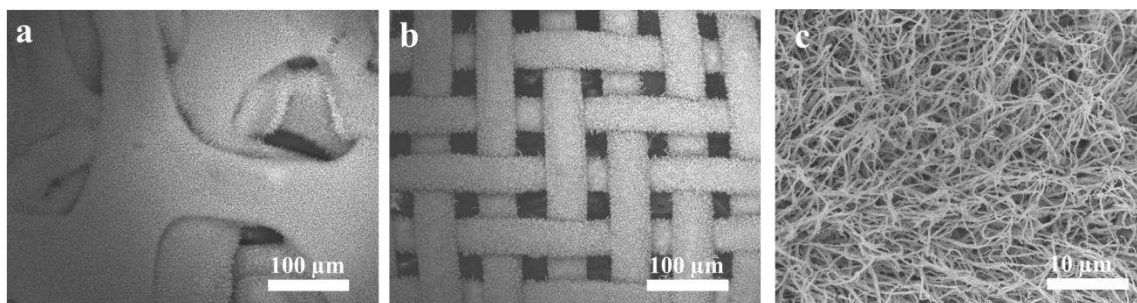Figure S4. a, b) SEM image of the CCG and CC electrode after 500 cycles, respectively.

Figure S5. SEM images of CCG coaxial nanowires grown on different substrates. a) Cu foam; b) Cu net; c) Cu foil.
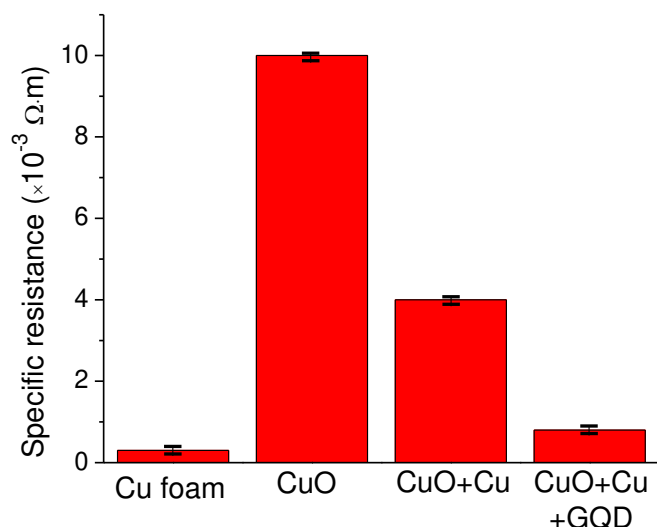
Determination of active material mass

The mass of all the samples after each step were weighed using an analytical balance (RADWAG, MYA 21, resolution: 1 µg) after a thorough and same condition of drying process. The mass of the sample after related steps were listed typically below in table 1.

Table S1. Mass of samples after related dealing steps

Steps	Dealing steps	Products after the step	Mass (mg)
0	Substrate after clean for CC	pure Cu foam	S_0=101.724
0'	Substrate after clean for CCG	pure Cu foam	$S_{0'}$=101.719
1	Cu foam after anodization (CC)	$Cu(OH)_2$ on Cu foam	S_1=102.534
1'	Cu foam after anodization (CCG)	$Cu(OH)_2$ on Cu foam	$S_{1'}$=102.529
2	Annealing in air (CC)	CuO on Cu foam	S_2=102.109
2'	Annealing in air (CCG)	CuO on Cu foam	$S_{2'}$=102.102
3'	Electrophoresis of GQDs	CuO+GQDs on Cu foam	$S_{3'}$=102.157
4	CuO annealing in $Ar+H_2$	CC on Cu foam	S_4=102.071
4'	CuO+GQDs annealing in $Ar+H_2$	CCG on Cu foam	$S_{4'}$=102.118

Based on the mass measurement above, we calculated the related mass for the samples as below:

(1) From step 0 to 2 (step 0' to 2'), the mass increase from Cu foam to CuO nanowires+Cu foam is due to the introducing of O, thus the mass of O gain is for CC sample is $m_O = S_2 - S_0 = 0.385$ mg while for CCG sample is $m_{O'} = S_{2'} - S_{0'} = 0.383$ mg. According to the comparison

$$Cu \rightarrow CuO$$
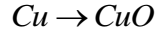
For CC sample, the mass of CuO can be determined as $m_{CuO} = m_O \times M_{CuO}/M_O = 0.385$ mg $\times 80/16 = 1.925$ mg

For CCG sample, the mass of CuO can be determined as $m_{CuO'} = m_{O'} \times M_{CuO}/M_O = 0.383$ mg $\times 80/16 = 1.915$ mg

(2) From step 2 to 4, the mass decrease can be understood as partial loss of O, the mass difference for CC anode is calculated as $\triangle m = S_2 - S_4 = 0.038$ mg, thus **the mass of active material for CC core-shell nanowires** is $m_{CC} = m_{CuO} - \triangle m = 1.925 - 0.038 = 1.887$ mg. The mass of CuO transferred to Cu layer is $m_{CuO\text{-}t} = \triangle m \times M_{CuO}/M_O = 0.038$ mg $\times 80/16 = 0.19$ mg, the ratio of CuO transferred is $r = m_{CuO\text{-}t}/m_{CuO} = 9.87\%$.

(3) From step 2' to step 3', the mass change is caused by adding GQDs, the mass of GQD is $m_{GQD} = S_{3'} - S_{2'} = 0.055$ mg. The O loss from step 3' to step 4' is $\triangle m' = S_{3'} - S_{4'} = 0.039$ mg, so the **mass of active materials of CCG coaxial nanowires** is $m_{CCG} = m_{CuO'} - \triangle m' + m_{GQD} = 1.931$ mg. The mass ratio of GQD layer of the CCG anode is $r' = m_{GQD}/m_{CCG} \approx 2.85\%$.

Reference

1. Y. Li, Y. Hu, Y. Zhao, G. Shi, L. Deng, Y. Hou and L. Qu, *Adv Mater*, 2011, **23**, 776-780.
2. D. Pan, J. Zhang, Z. Li and M. Wu, *Adv Mater*, 2010, **22**, 734-738.
3. H. Hagemann, H. Bill, W. sadowski, E. Walker and M. François, *Solid State Commun.*, 1990, **73**, 447-451.
4. H. F. Goldstein, D.-s. Kim, P. Y. Yu, L. C. Bourne, J. P. Chaminade and L. Nganga, *Phys. Rev. B*, 1990, **41**, 7192-7194.
5. T. Yu, X. Zhao, Z. X. Shen, Y. H. Wu and W. H. Su, *J. Cryst. Growth*, 2004, **268**, 590-595.
6. M. H. Chou, S. B. Liu, C. Y. Huang, S. Y. Wu and C. L. Cheng, *Appl. Surf. Sci.*, 2008, **254**, 7539-7543.
7. R. Hawaldar, P. Merino, M. R. Correia, I. Bdikin, J. Grácio, J. Méndez, J. A. Martín-Gago and M. K. Singh, *Sci. Rep.*, 2012, **2**.
8. W. Wang, Q. Zhou, X. Fei, Y. He, P. Zhang, G. Zhang, L. Peng and W. Xie, *CrystEngComm*, 2010, **12**, 2232-2237.
9. D. R. Dreyer, S. Park, C. W. Bielawski and R. S. Ruoff, *Chem. Soc. Rev.*, 2010, **39**, 228-240.
10. D. Yang, A. Velamakanni, G. Bozoklu, S. Park, M. Stoller, R. D. Piner, S. Stankovich, I. Jung, D. A. Field, C. A. Ventrice Jr and R. S. Ruoff, *Carbon*, 2009, **47**, 145-152.